Supporting Information

Hydrogen Evolution with Nanoengineered ZnO Interfaces Decorated by a Beetroot Extract and a Hydrogenase Mimic

M. V. Pavliuk,[a] A. M. Cieślak,[b] M. Abdellah,[a] A. Budinská,[a] S. Pullen,[a] K. Sokołowski,[b] D. L. A. Fernandes,[a] J. Szlachetko,[b] E. L. Bastos,[c] S. Ott,[a] L. Hammarström,[a] T. Edvinsson,[a] J. Lewiński[b, d, *] and J. Sá[a, c, *]

1. Experimental

All reagents were purchased from commercial vendors (Sigma Aldrich and ABCR GmbH) and used as received. All spectroscopic and catalysis experiments were performed in DMSO (solvent), ensuring that the same conditions were used for the spectroscopies and catalysis. The DMSO was used without any purification or drying. Water-soluble ZnO NCs were prepared according to the developed organometallic synthetic approach [S1]. For the synthesis we employed 2,5,8,11-tetraoxatetradecan-14-oic acid (MeO EG_3 COOH; denoted as OEG-H) as oligoethylene glycol proligand, which formed the carboxylate stabilizing shell of ZnO-OEG NCs. The catalyst used in this study, [FeFe](mcbdt)$(CO)_6$, was synthesized according to [S2].

ZnO-OEG NCs were sensitized with betanin, a natural organic dye [S3], and a proton reduction catalyst, inspired by the active site structure of [FeFe]-hydrogenase, yielding the surface modified ZnO-OEG-B-Cat NCs. At first 50.5 mg of betanin (Sigma Aldrich) were dissolved in 1 mL of DMSO. Resulted pinkish-red solution was added to 40 mg of ZnO-OEG NCs and sonicated for 5 min to further provide uniform orange-yellow dispersion. UV-Vis spectra were monitored until no further changes were observed. Afterwards this suspension was used to dissolve 1.48mg of [FeFe](mcbdt)$(CO)_6$. During photocatalytic studies 3 drops of trifluoracetic acid was added to the reaction mixture. HRTEM, DLS and ^{1}H NMR spectroscopy were used to monitor the core morphology, hydrodynamic diameter as well as organic shell composition of ZnO-OEG-B-Cat NCs (Figure S4-6). The data show that both betanin and catalyst are bound to the NCs' surface and the surface modification did not affect the core size and its crystallinity. Additional UV-Vis, SSIR spectroscopic measurements were

used to confirm sensitization of ZnO-OEG NCs with betanin and [FeFe](mcbdt)$(CO)_6$ (Figure S1-S2).

1.1 Steady-state absorption and IR spectroscopy

Absorption spectra were measured on a Varian Cary 5000. Infrared (IR) spectra were recorded in a modified Omni cell (Specac) with O-ring sealed CaF_2 windows and a path length of 500 μm using a Bruker IFS 66v/S FTIR spectrophotometer controlled with OPUS software.

1.2. Transient absorption IR-spectroscopy

For transient absorption measurements a frequency doubled Q-switched Nd:YAG laser (Quanta-Ray ProSeries, Spectra-Physics) was employed to obtain 532 nm pump light, 10 mJ/pulse with a FWHM of 10 ns. Probing was done with the continuous wave quantum cascade (QC) IR laser with a tuning capability between 1960–2150 cm^{-1} (Daylight Solutions). For IR detection a liquid nitrogen-cooled mercury-cadmium-telluride (MCT) detector (KMPV10-1-J2, Kolmar Technologies, Inc,) was used. The IR probe light was overlapped with the actinic laser beam in a quasi co-linear arrangement at 25° angle. Transient absorption traces were acquired with a Tektronix TDS 3052 500 MHz (5GS/s) oscilloscope in connection with the L900 software (Edinburgh Instruments) and processed using Origin 9 software. Samples were kept in a modified Omni cell (Specac) with with O-ring sealed CaF_2 windows and a path lenth of 500 μm.

1.3. Ultrafast transient mid-infrared absorption spectroscopy

The 1 mJ, 45 fs output of a 1 kHz Ti:Sapphire amplifier (Spitfire Pro, Spectra-Physics) was split into two separate commercial optical para-metric amplifiers (TOPAS-C, Light Conversion), which generate the visible pump 530 nm and the mid-IR probe (1850–2200 cm^{-1}) pulses. Prior to reaching the sample, the probe beam was split into equal intensity probe and reference beams using a wedged ZnSe window. Both beams pass through the sample, but only the probe beam interacts with the photoexcited volume. All beams are focused with a single f = 10 cm off axis parabolic mirror to a ~70 μm spot size in the sample. The pump intensity was attenuated to 250 μW. The probe and reference beams were dispersed by a commercial monochromator (Triax 190, HORIBA Jobin Yvon) equipped with a 75 groove/mm grating and detected on a dual array, 2x64 pixel mercury cadmium telluride detector (InfraRed Associated, Inc). The instrument response function for the experiments was approximately

100 fs. The sample was mounted in a Harrick flow cell, which gave a sample thickness of roughly 500 µm.

1.4. Theoretical calculations

The quantum chemical calculations were performed in the Gaussian 09 package [S4] using hybrid density functional theory (DFT) on a B3LYP/6-311G(d,p) level in gas phase and a polarizable continuum model (PCM) solvent model. Self-consistent reaction field where used with the surrounding dielectric media of DMSO incorporated using the molecular structure of DMSO from the United Atom Topological Model (UAKS) (based on radii from a PBE1PBE/6-31G(d) level of theory). The theoretical IR vibrations were obtained from linear response calculations were performed on the ground state optimized structures within the PCM solvent model and using the dielectric constant of DMSO corresponding to 298 K.

2. Characterization of ZnO-OEG NCs with betanin and [FeFe](mcbdt)$(CO)_6$

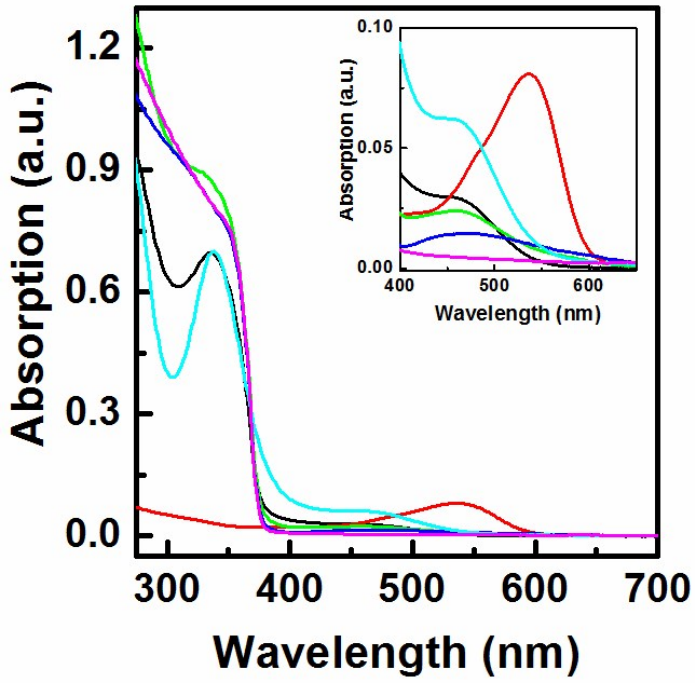

Figure S1. Absorption spectra in DMSO of: (a) ZnO-OEG NCs *(purple line)*; (b) betanin *(red line)*; catalyst [FeFe](mcbdt)$(CO)_6$ *(cyan line)*; betanin functionalized ZnO-OEG-B NCs *(blue line)*; catalyst functionalized ZnO-OEG-Cat NCs *(black line)*; and both betanin and catalyst functionalized ZnO-OEG-B-Cat NCs *(green line*

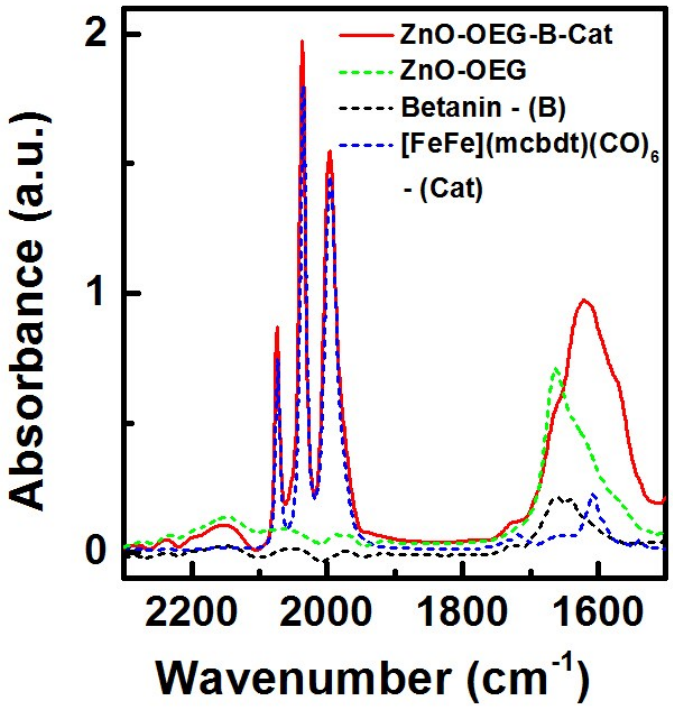

Figure S2. FTIR spectra of betanin *(black dotted line)*; ZnO-OEG NCs *(green dashed line)* catalyst [FeFe](mcbdt)$(CO)_6$ *(blue dashed line)*; and both betanin and catalyst functionalized ZnO-OEG-B-Cat NCs *(red line)* in DMSO.

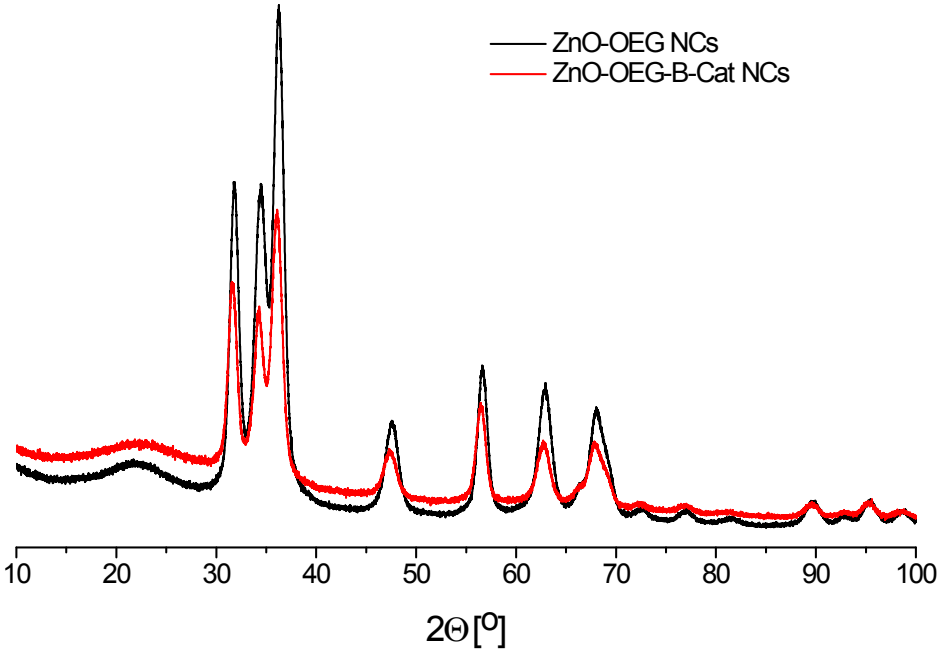

Figure S3. The PXRD diffractogram of ZnO-OEG NCs *(black line)* and nano-hybrid ZnO-OEG-B-Cat system *(red line)*. Based on the reflection broadening, according to the Scherrer equation, the ZnO crystallite size has been estimated to be 6.5 ± 0.4nm and 6.9 ± 0.5 nm, respectively.

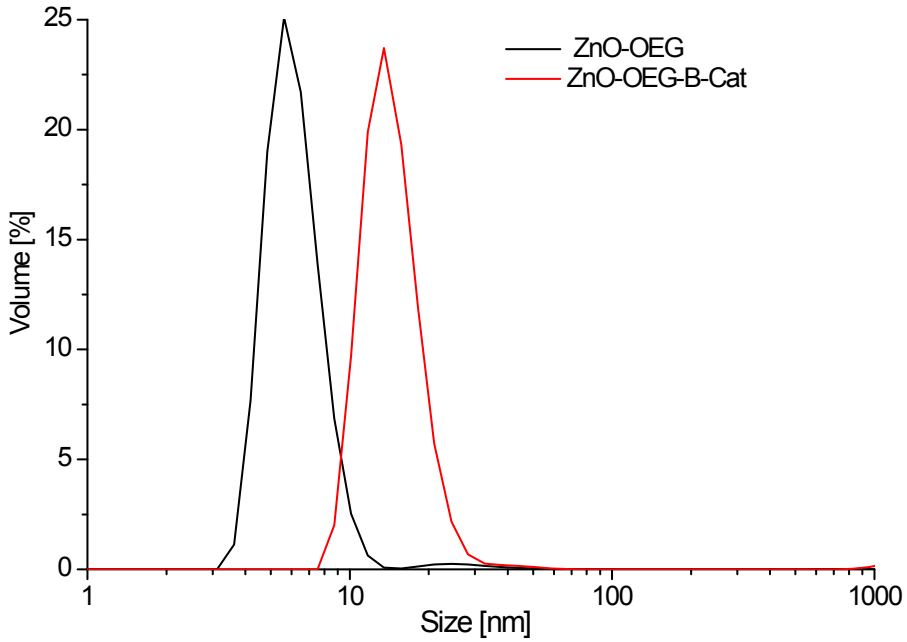

Figure S4. The average hydrodynamic diameter 7 ± 2 nm of ZnO-OEG NCs and 13 ± 2 nm of nano-hybrid ZnO-OEG-B-Cat system in DMSO estimated by DLS.

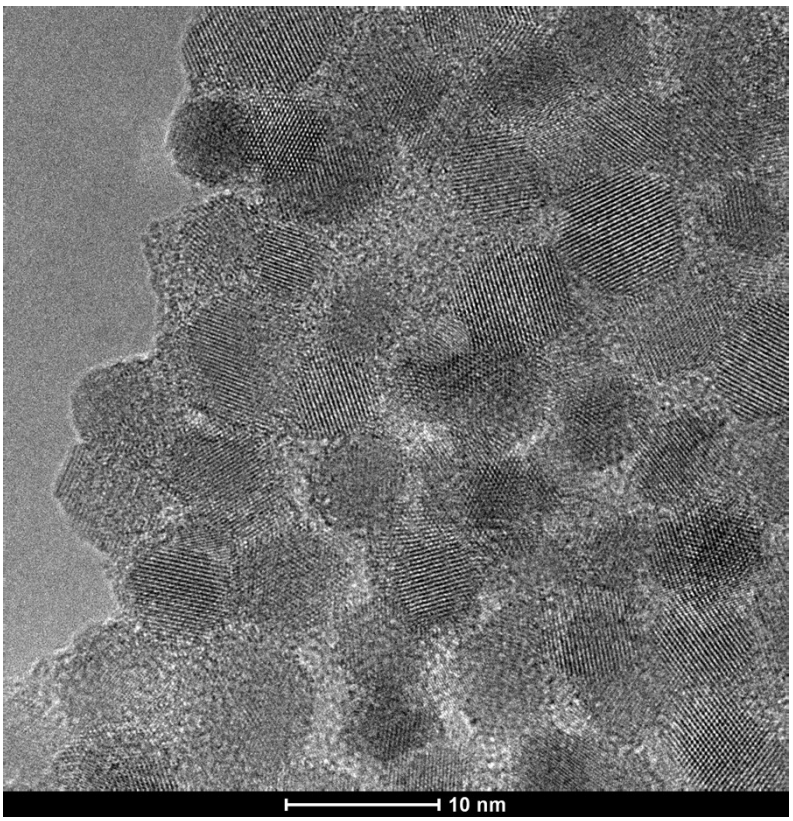

Figure S5. The HRTEM image of nano-hybrid ZnO-OEG-B-Cat system drop-casted from DMSO solution.

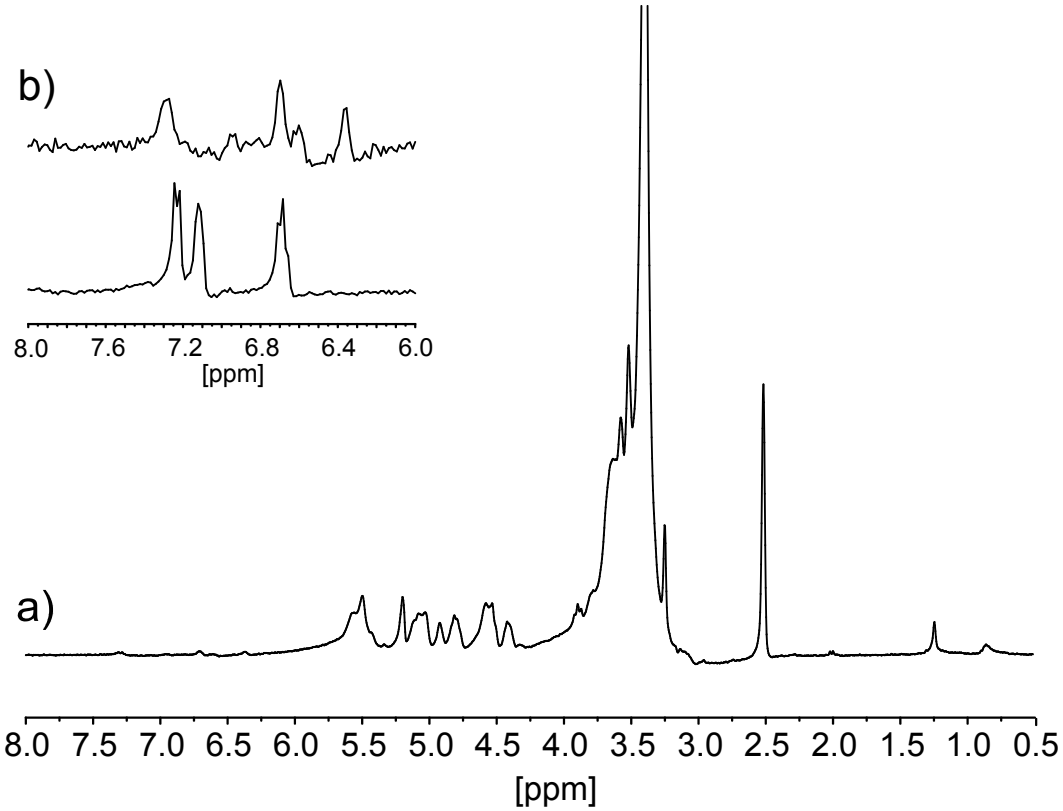

Figure S6. ^{1}H NMR analysis (300 MHz, d-DMSO, 25 °C) of nano-hybrid ZnO-OEG-B-Cat system (*a*). The inset (*b*) shows that in the ^{1}H NMR spectrum of ZnO-OEG-B-Cat system (*top spectrum*) the signals of the *mcbdt* attributed to protons of benzanoic ring are clearly broadened and shifted in comparison to the corresponding free *mcbdt* (δ = 7.25, 7.15 and 6.7 ppm; *bottom spectrum*). This suggests that the catalyst molecules are bound to Zn centres on the ZnO surface via the carboxylic group of the benzoic ring.

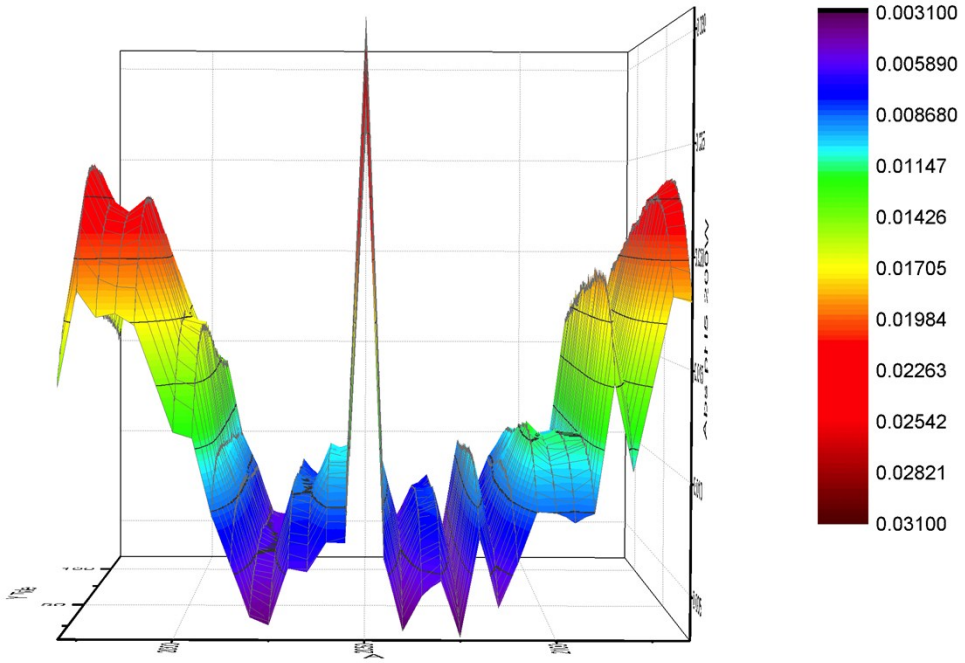

Figure S7. 3D surface plot of transient IS absorption spectrum of $[ZnO\text{-}OEG\text{-}B\text{-}Cat]^-$ NCs during excitation at 532 nm in DMSO different xyz prespective of figure 2a.

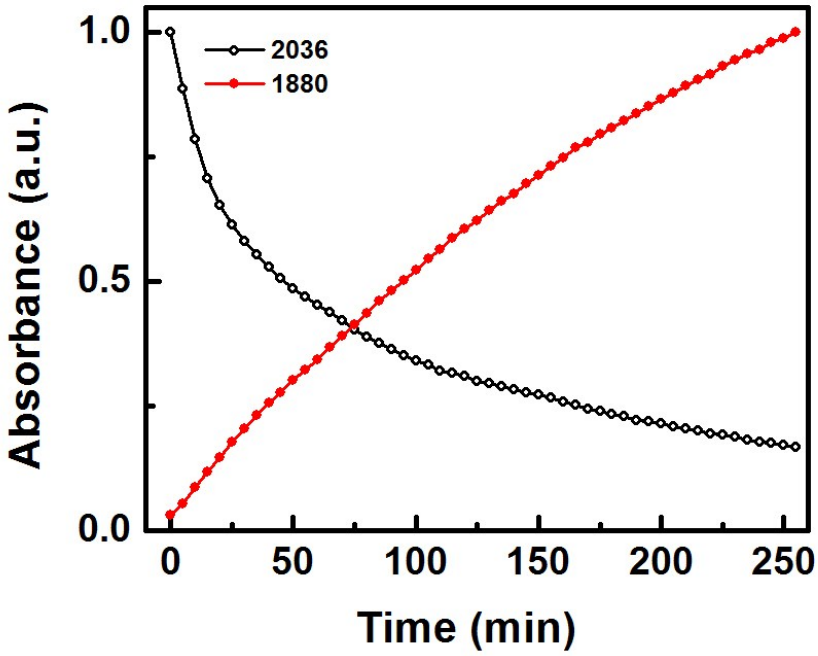

Figure S8. Kinetic traces of 2036 and 1880 cm^{-1} IR bands, extracted from steady-state IR measurements.

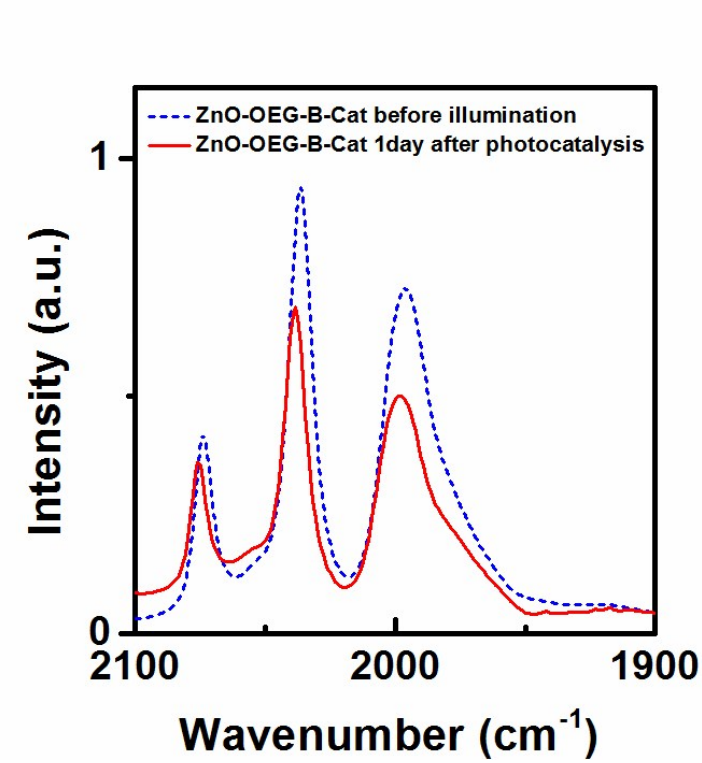

Figure S9. IR absorption specta of ZnO-OEG-B-Cat NCs before illumination at 532 nm in DMSO (*blue dashed line*) and 1 day after photocatalysis (*red line*).

Table S1. Bond lengths calculated with DFT (distances in Å)

	Gas_phase FeFe](mcbdt)$(CO)_6$	**FeFe](mcbdt)$(CO)_6^{-1}$**	**FeFe](mcbdt)$(CO)_6^{-2}$**
Fe_1-Fe_2	**2.437**	**2.635**	**3.497**
Fe_1-S_1	**2.315**	**2.333**	**2.417**
Fe_1-S_2	**2.315**	**2.333**	**2.502**
Fe_2-S_1	**2.324**	**2.443**	**2.417**
Fe_2-S_2	**2.324**	**2.443**	**2.502**
S_1-S_2	**3.021**	**3.079**	**2.998**
Fe-C	**1.791 (1.789)**	**1.802 (1.773)**	**1.745 (1.756)**

Table S2. Summary of the vibrations for the various catalyst species using linear response DFT using DMSO in a PCM solvent model

Experimental data for ZnO-OEG-B-Cat in DMSO				
	ν_{C-O} (cm^{-1})			***Additional bands***
Before illumination	2074	2036	1996	
2μs after illumination	2050 (24)	1985 (51)	-	
4h 10 min after illumination	2000 (74), 1974 (100)	1880 (157)	1825 (171)	1914 (160)
Theoretical data for [FeFe](mcbdt)$(CO)_6$ in DMSO (Solvent model)				
	ν_{C-O} (cm^{-1})			***Additional bands***
[FeFe](mcbdt)$(CO)_6$	2138	2075	2038/2047	
[FeFe](mcbdt)$(CO)_6^-$	2067	1975/1945	1922	
[FeFe](mcbdt)$(CO)_6^{2-}$	1998/1979	1874	1842/1830	1691 (Bridged CO stretch)

*Information in brackets is the difference between band position values before and after illumination.

Table S3. Summary of the bond length for the various catalyst species within the DMSO PCM solvent model

Bond type	**Distance (Å)**		
	[FeFe](mcbdt)$(CO)_6$	[FeFe](mcbdt)$(CO)_6^-$	[FeFe](mcbdt)$(CO)_6^{2-}$
Fe_1–Fe_2	2.442	2.663	3.464
Fe_1–S_1	2.314	2.382	2.478
Fe_1–S_2	2.314	2.376	2.407
Fe_2–S_1	2.324	2.357	2.413
Fe_2–S_2	2.324	2.420	2.485
S_1–S_2	3.011	3.071	2.984
Fe–C	1.788	1.801 (1.765)	1.751 (1.744)

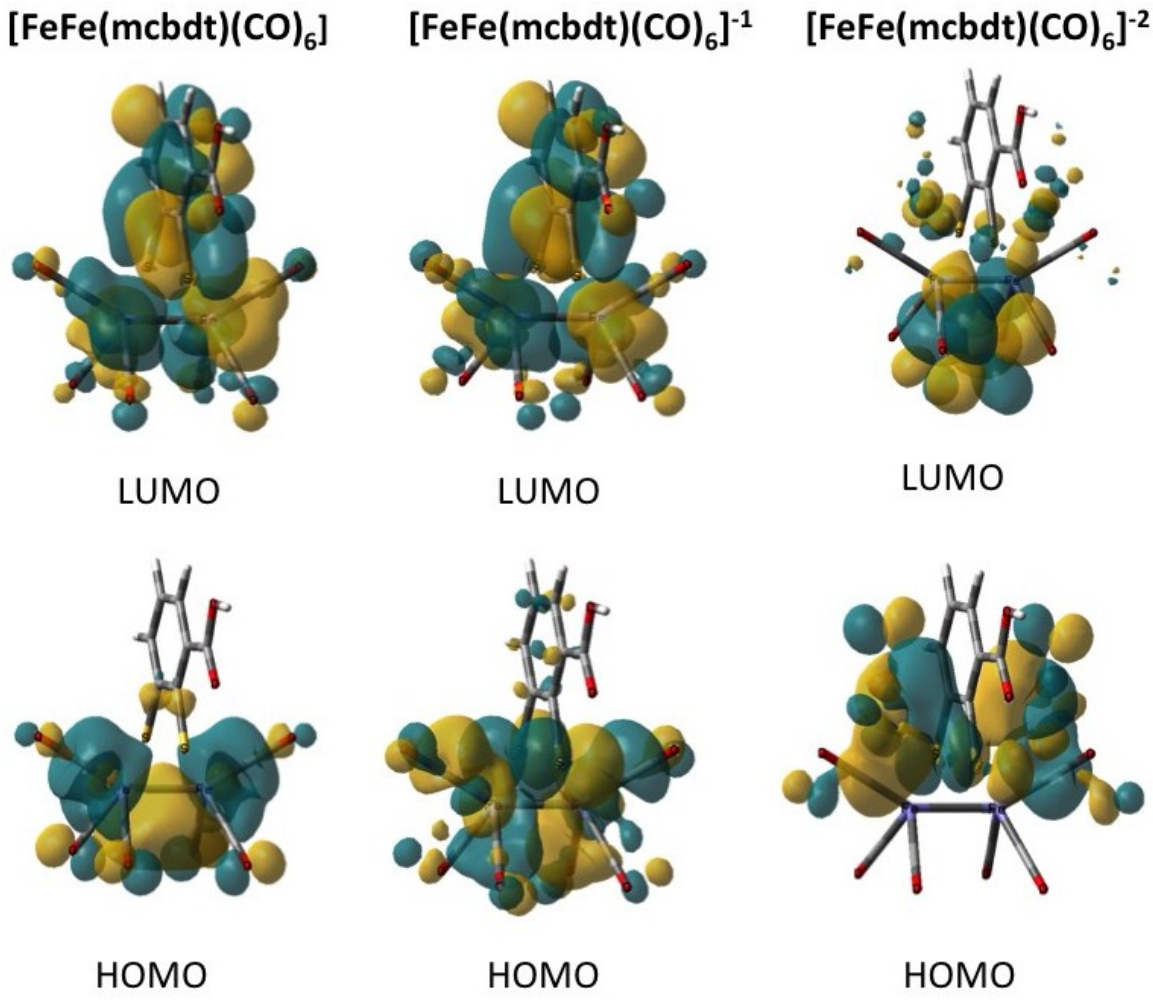

Figure S10. HOMO and LUMO for the neutral and different reduced states of the catatalyst.

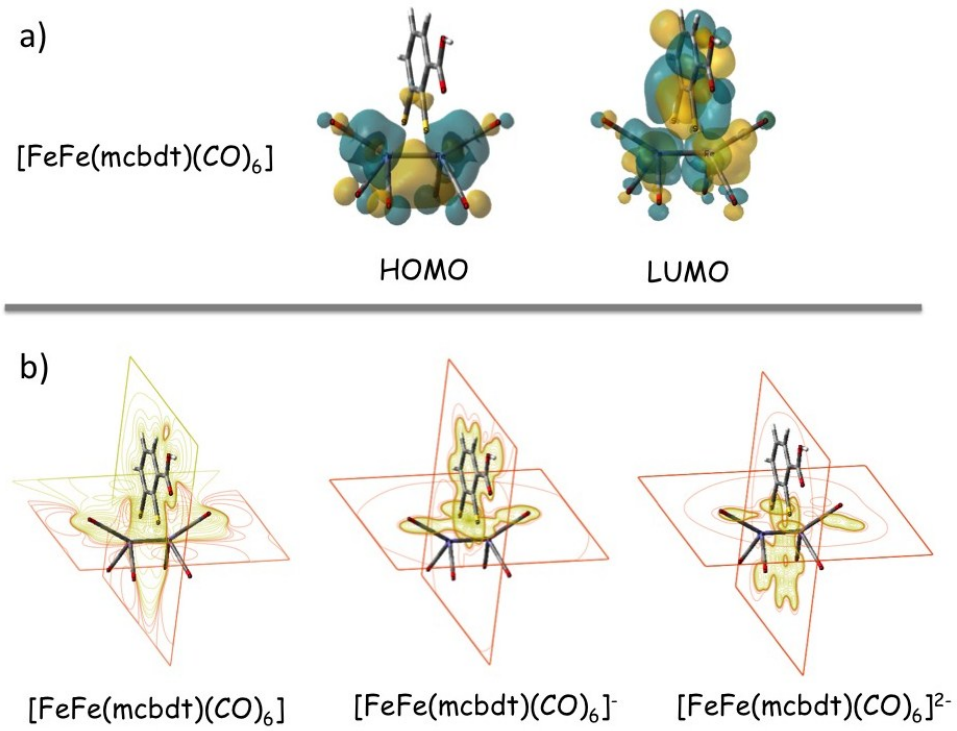

Fig. S11 a) HOMO and LUMO orbitals of the unreduced [FeFe(mcbdt)(CO)$_6$]. b) Electrostatic contour 30x30 Å and in *xy*-plane and *zx*-plane showing a redistribution of charge in between the Fe-Fe and towards the lower pointing oxygens in the CO-groups upon reduction.

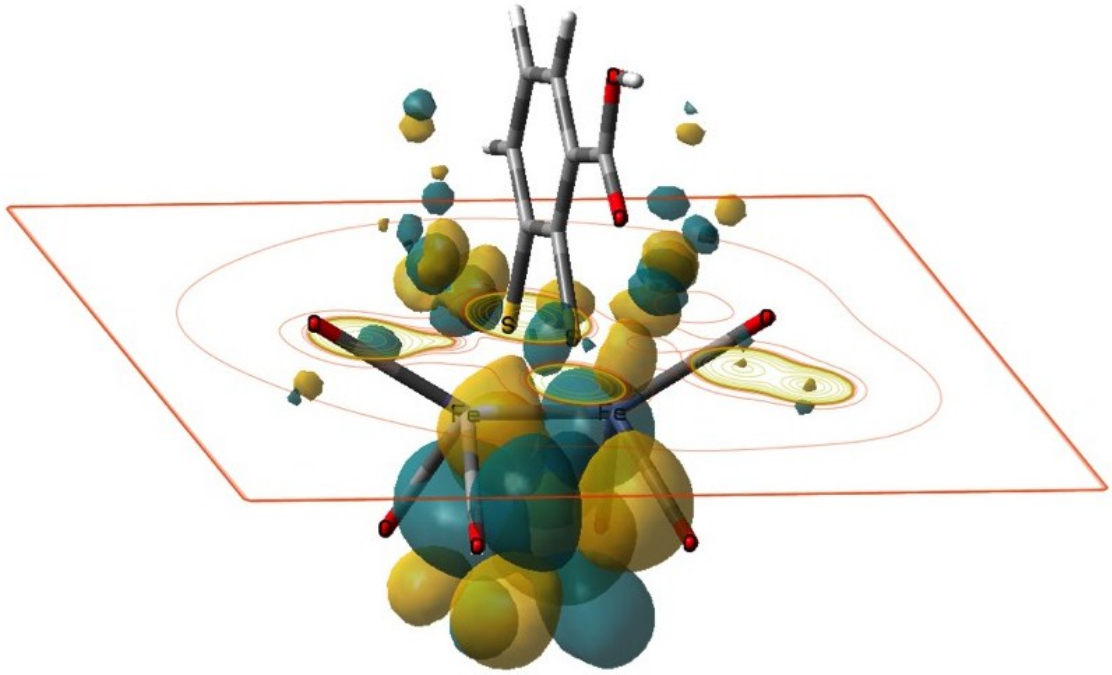

Figure S12. [FeFe(mcbdt)(CO)$_6$]$^{-2}$ LUMO + Electrostatic contour 30x30 Å in the xy-plane

References

[S1] A. M. Cieślak, E.-R. Janeček, K. Sokołowski, T. Ratajczyk, M. K. Leszczyński, O. A. Scherman, J. Lewiński, Reversible light modulation of cucurbit[8]urils host−guest systems through photoactive water-soluble ZnO nanocrystals, submitted to Angewandte Chemie no. 201604116.

[S2] A. M. Brown, L. Antila, M. Mirmohades, S. Pullen, S. Ott, L. Hammarström, Ultrafast Electron Transfer Between Dye and Catalyst on a Mesopo-rous NiO Surface, *J. Am. Chem. Soc.*, **2016**, *138*, 8060–8063.

[S3] a) L. C. P. Gonçalves, S. M. Silva, P. C. DeRose, R. A. Ando, E. L. Bastos, Plos One, 8 (2013) e73701; b) L. C. P. Gonçalves, R. R. Tonelli, P. Bagnaresi, R. A. Mortara, G. A. Ferreira, E. L. Bastos, Plos One, **2013**, *8,* e53874.

[S4] *Gaussian 09*, Revision A.01, M. J. Frisch, G. W. Trucks, H. B. Schlegel, G. E. Scuseria, M. A. Robb, J. R. Cheeseman, G. Scalmani, V. Barone, B. Mennucci, G. A. Petersson, H. Nakatsuji, M. Caricato, X. Li, H. P. Hratchian, A. F. Izmaylov, J. Bloino, G. Zheng, J. L. Sonnenberg, M. Hada, M. Ehara, K. Toyota, R. Fukuda, J. Hasegawa, M. Ishida, T. Nakajima, Y. Honda, O. Kitao, H. Nakai, T. Vreven, J. A. Montgomery, Jr., J. E. Peralta, F. Ogliaro, M. Bearpark, J. J. Heyd, E. Brothers, K. N. Kudin, V. N. Staroverov, R. Kobayashi, J. Normand, K. Raghavachari, A. Rendell, J. C. Burant, S. S. Iyengar, J. Tomasi, M. Cossi, N. Rega, J. M. Millam, M. Klene, J. E. Knox, J. B. Cross, V. Bakken, C. Adamo, J. Jaramillo, R. Gomperts, R. E. Stratmann, O. Yazyev, A. J. Austin, R. Cammi, C. Pomelli, J. W. Ochterski, R. L. Martin, K. Morokuma, V. G. Zakrzewski, G. A. Voth, P. Salvador, J. J. Dannenberg, S. Dapprich, A. D. Daniels, Ö. Farkas, J. B. Foresman, J. V. Ortiz, J. Cioslowski, and D. J. Fox, Gaussian, Inc., Wallingford CT, 2009.